SMCHD1 loss triggers DUX4 expression by disrupting splicing in FSHD2

Eden Engal[1,2,3], Aveksha Sharma[2], Nadeen Taqatqa [2], Mercedes Bentata[1,2], Shiri Jaffe-Herman[2], Ophir Geminder[2], Reyut Lewis[1], Marc Gotkine[4], Maayan Salton[2,*] and Yotam Drier[1,*]

[1] The Lautenberg Center for Immunology and Cancer Research, The Institute for Medical Research Israel-Canada, Faculty of Medicine, The Hebrew University of Jerusalem, Jerusalem 9112102, Israel

[2] Department of Biochemistry and Molecular Biology, The Institute for Medical Research Israel-Canada, Faculty of Medicine, The Hebrew University of Jerusalem, Jerusalem 9112102, Israel

[3] Department of Military Medicine and "Tzameret", Faculty of Medicine, The Hebrew University of Jerusalem, Jerusalem 9112102, Israel

[4] Department of Neurology, Hadassah Medical Organization and Faculty of Medicine, Hebrew University of Jerusalem, Jerusalem 9112102, Israel

* To whom correspondence should be addressed: maayan.salton@mail.huji.ac.il, yotam.drier@mail.huji.ac.il

Running head: SMCHD1 induces DUX4 by disrupting splicing in FSHD2

Keywords: SMCHD1, facioscapulohumeral muscular dystrophy, pre-mRNA splicing, transcription elongation, RBM5

Abstract

Structural Maintenance of Chromosomes Flexible Hinge Domain Containing 1 (SMCHD1) is a non-canonical member of the structural maintenance of chromosomes (SMC) protein family involved in the regulation of chromatin structure, epigenetic regulation and transcription. Mutations in SMCHD1 cause facioscapulohumeral muscular dystrophy type 2 (FSHD2), a rare genetic disorder characterized by progressive muscle weakness and wasting, believed to be caused by aberrant expression of DUX4 in muscle cells. Here we suggest a new role for SMCHD1 as a regulator of alternative splicing, and demonstrate how splicing alteration caused by SMCHD1 mutations can lead to DUX4 expression and FSHD pathogenesis. Analyzing RNA-seq data from muscle biopsies of FSHD2 patients and FSHD2 mouse model we found that hundreds of genes were mis-spliced upon SMCHD1 mutation. At least 20% of mis-spliced genes were associated with abnormalities of the musculature. Moreover, we show that mis-spliced exons tend to be bound by SMCHD1, and SMCHD1 bound exons demonstrate slower elongation rate, suggesting SMCHD1 binding promotes exon exclusion by slowing RNA polymerase II (RNAPII). Specifically, we discovered that SMCHD1 mutations promotes the splicing of the DNMT3B1 isoform of DNMT3B by perturbing RNAPII elongation rate and recruitment of the splicing factor RBM5. The mis-splicing of DNMT3B leads to hypomethylation of the D4Z4 region and to DUX4 overexpression. These results suggest that mis-splicing by SMCHD1 may play a major role in FSHD2 pathogenesis by promoting mis-splicing of different targets including DNMT3B, and highlight the potential for targeting splicing as a therapeutic strategy for this disorder.

Significance statement

Our study sheds light on how loss of SMCHD1 drives pathogenesis of facioscapulohumeral muscular dystrophy (FSHD), a genetic disorder characterized muscle atrophy. We found that SMCHD1 mutations led to changes in splicing of hundreds of genes, 20% of which related to muscle abnormalities. We found that SMCHD1 bound exons typically exhibit slower elongation rate of RNA polymerase II and exon exclusion, and are mis-spliced upon SMCHD1 loss. One of these targets is the DNA Methyltransferase DNMT3B, where the isoform promoted by SMCHD1 loss leads to hypomethylation of a repeat region near DUX4 and to DUX4 overexpression, a known cause for FSHD. Our results provide insight into the molecular mechanisms underlying this disorder, and suggest splicing modulation as a therapeutic strategy.

Introduction

Splicing of precursor mRNA (pre-mRNA) is a key regulatory process in gene expression. While splicing is the process in which exons are joined together, alternative splicing is the process in which different exons are spliced together in a combinatorial fashion, either including or excluding an exon from the final transcript. Thus, alternative pre-mRNA splicing enables the construction of distinct protein isoforms from the same gene and contributes to the cell's diverse protein population. Proper splicing is necessary for the cell's function and when altered may lead to several pathological processes such as cancer and genetic diseases[1,2]. As an essential regulatory process in the cell, alternative splicing is tightly regulated. Many factors can regulate alternative splicing, including cis-acting elements within the pre-mRNA molecule and trans-acting factors, mostly splicing factors, proteins that alter splicing by regulating splice site selection.

Another trans acting factor regulating alternative splicing is RNA polymerase II (RNAPII). Typically, slow RNAPII elongation kinetics promotes exon inclusion, as it exposes additional splice sites[3]. Therefore, altering elongation rate by replacing a gene's promoter or altering its chromatin can impact splicing[4]. In some cases, the opposite effect is observed whereby slow RNAPII kinetics promotes exon exclusion[5]. This effect was attributed to an inhibitory splicing factor that is recruited by RNAPII Carboxy-terminal domain (CTD) and gains a binding opportunity when RNAPII is slow to transcribe[5]. Several chromatin modulators have previously been shown to act as regulators of splicing, including the architectural regulator CCCTC-binding factor (CTCF), that regulate splicing via changes in RNAPII elongation rate[6,7].

In our previous work, we conducted an unbiased high-throughput screen to identify chromatin regulators with a role in modulating alternative splicing[8,9]. Our results identified 16 chromatin proteins associated with alternative splicing regulation, including the structural maintenance of chromosomes flexible hinge domain-containing 1 (SMCHD1) protein[8]. SMCHD1 is an SMC protein comprising an N-terminal GHKL (gyrase, Hsp90, histidine kinase, MutL) ATPase domain and an SMC (structural maintenance of chromosomes) hinge domain that possesses chromatin-binding activity[10]. As an SMC protein, SMCHD1 function is speculated to contribute to the maintenance of DNA and chromatin structure. SMCHD1 knockout has previously presented significant effects on histone modifications, DNA methylation, CTCF occupancy and chromosomal interactions[10–16]. SMCHD1 was also shown to play a key role in the X inactivation process and in the silencing of autosomal genes[10].

A variety of heterozygous loss-of-function mutations in the SMCHD1 gene have been described to cause facioscapulohumeral dystrophy type 2 (FSHD2), a late-onset progressive muscular dystrophy disease[17]. The suggested molecular basis of FSHD2 is hypomethylation of the D4Z4 macrosatellite array, caused by SMCHD1 loss of function. This results in higher expression of the DUX4 transcription factor and myocyte toxic genes[18]. FSHD1 is caused by contractions of the D4Z4 macrosatellite array, associated with loss of methylation at this site and is more common than FSHD2[19]. While most FSHD cases that are not attributed to D4Z4 contraction are caused by SMCHD1 mutations, FSHD has also been described in patients with mutations in the DNA Methyltransferase 3 Beta (DNMT3B) gene (FSHD4) and the Ligand Dependent Nuclear Receptor Interacting Factor 1 (LRIF1) gene (FSHD3)[20,21]. Both SMCHD1 and DNMT3B variants have been identified as modifiers of disease severity in FSHD1 patients as well[20,22,23]. In addition, missense mutations in the ATPase domain of SMCHD1 were demonstrated to cause bosma arhinia microphthalmia syndrome (BAMS), a rare condition characterized by severe facial abnormalities, especially in the nasal area. The underlying molecular basis of the disease is not well understood[24–26].

Here we describe a novel role for SMCHD1 as a regulator of alternative splicing. We studied genome-wide alternative splicing, in neural stem cells of mice with SMCHD1 mutations as well as muscle of FSHD2 patients. We found aberrantly spliced genes to be bound by SMCHD1 on the DNA level and to be enriched for FSHD pathology. Our results show that binding of SMCHD1 to abnormally spliced genes is associated with RNAPII pause sites. In particular, we focus on DNMT3B and demonstrate that SMCHD1 mutations lead to preferential inclusion of exons 5, 21 and 22, and expression of the full DNMT3B isoform instead of shortened DNMT3B3ΔEx5 isoform. We show that expression of the full isoform instead of DNMT3B3ΔEx5 leads to hypomethylation of the D4Z4 repeat array and promotes DUX4 expression, the key events causing FSHD. Therefore, we suggest a new model for FSHD2 pathogenesis, driven by SMCHD1 mediated alternative splicing.

Results

Differential splicing in FSHD2 patients with SMCHD1 mutation

To explore alternative splicing in SMCHD1 mutated FSHD2 patients, we compared RNA-seq data of muscle biopsies of four FSHD2 patients with mutations in the SMCHD1 gene with four healthy individuals[18]. While 117 genes are differentially expressed (FDR < 5%, DESeq2), at least 871 genes are mis-spliced (FDR < 5%, rMATS). 1420 mis-splicing events were identified, 46%

of them are exon skipping events (649 events) (Fig. 1A). The other 54% are composed of different alternative splicing events including mutually exclusive exons (407 events), intron retention (124 events), alternative 3' splice site (97 events) and alternative 5' splice site (143 events). Interestingly, only eight genes were identified as both differentially expressed and alternatively spliced, suggesting that SMCHD1 independently regulates gene expression and splicing (Fig. 1B). In order to control for splicing changes that are independent of SMCHD1 mutations, we repeated the analysis comparing FSHD2 patients to FSHD1 patients and discovered 1968 splicing events in 845 genes (FDR < 5%, rMATS). Importantly, 253 of these genes (30%) are the same genes detected in the comparison to healthy individuals ($p < 0.00001$, Fisher exact test, Fig. 1C). Overall, these results reveal significant mis-splicing in SMCHD1 mutated FSHD2 patients, pointing to a role for SMCHD1 in alternative splicing.

We next asked how splicing alteration by SMCHD1 can contribute to the phenotype of FSHD2. To this end, we explored the function of genes regulated in splicing by gene-set enrichment analysis. 20% (175 genes of 871, FDR < $4.2*10^{-7}$) of the genes mis-spliced in FSHD2 patients are associated with "abnormality of the musculature" annotation by the Human Phenotype Ontology (HPO[44]), suggesting that many genes mis-spliced due to SMCHD1 mutations in FSHD2 are associated with abnormal muscle function. Top significant enriched human phenotype terms included many annotations associated with muscular dystrophy which are related to FSHD2 pathology (Fig. 1D). Analysis of genes differentially spliced between FSHD2 and FSHD1 yielded similar results. However, gene-set enrichment analysis of differentially expressed genes revealed no enrichment for FSHD-related phenotypes.

SMCHD1 regulates alternative splicing in mice neural stem cell and embryonic fibroblasts

To further investigate potential genes whose splicing is regulated by SMCHD1, we conducted deep sequencing of RNA from neural stem cell (NSC) sorted from Smchd1 null mice. The Smchd1^{MommeD1} mice are a previously established model with a mutation in one allele of Smchd1, resulting in Smchd1 haploinsufficeny[10]. Here, we compared MommeD1 homozygous NSCs to WT controls, to measure aberrant splicing in the absence of Smchd1. Differential splicing analysis identified 1075 splicing events in 860 genes (FDR < 5%, rMATS). 49% of the splicing events due to Smchd1 loss are exon skipping events (530 events) (Fig. 1E). The other 51% are composed of different splicing events including mutually exclusive exons (50 events), intron retention (205 events), alternative 3' splice site (166 events) and alternative 5' splice site (124 events). 59% of these events presented higher inclusion in Smchd1^{MommeD1} samples and 41% presented higher exclusion, suggesting Smchd1 is regulating splicing in both directions. We identified only 82 differentially expressed genes (DESeq2, FDR < 5%) and only

Figure 1

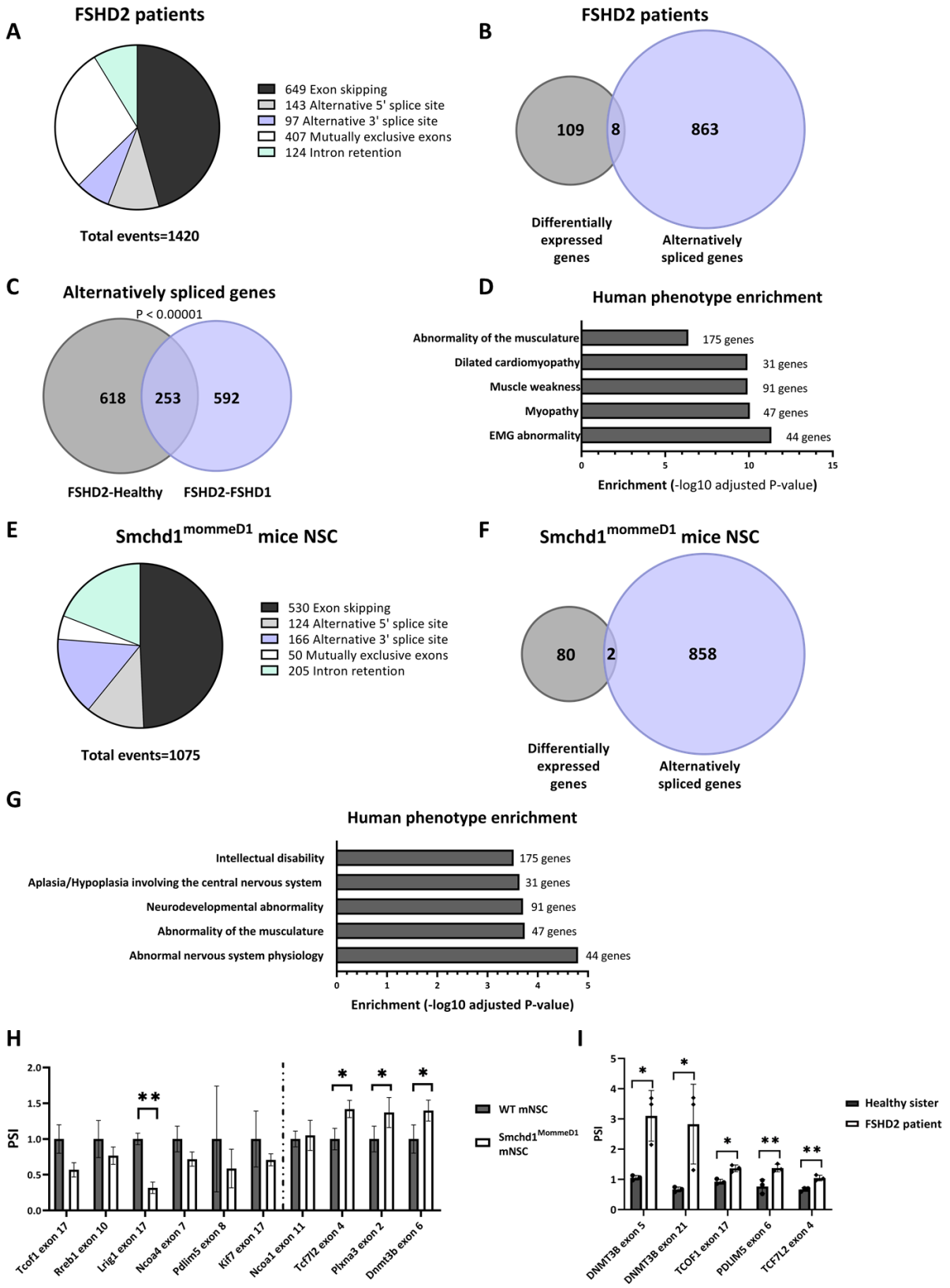

Figure 1: SMCHD1 is a regulator of alternative splicing. **(A-D)** Significant alternative splicing in muscles of FSHD2 patients revealed by rMATS analysis of RNA-seq data from healthy, FSHD1 and FSHD2 patients (ref 18). **(A)** Proportion of each alternative splicing event between muscles of FSHD2 patients and healthy individuals. **(B)** Venn diagram presenting the overlap between differentially expressed and alternatively spliced genes in FSHD2 patients. **(C)** Venn diagram presenting the overlap of alternative splicing events when FSHD2 patients are compared to FSHD1 patients or to healthy individuals. **(D)** Human phenotypes gene set enrichment of FSHD2 alternatively spliced genes, bars present -$\log_{10}$ adjusted p value, number of alternatively spliced genes are annotated next to bar. **(E-H)** Significant alternative splicing in Smchd1 null neural stem cells revealed by rMATS analysis of RNA-seq from three Smchd1 null and two WT mice NSC samples. **(E)** Proportion of each alternative splicing event is presented relative to WT. **(F)** Venn diagram presenting the overlap between Smchd1 expressed and alternatively spliced genes in Smchd1 null mice NSC. **(G)** Human phenotypes gene set enrichment of Smchd1 null alternatively spliced genes, bars present -$\log_{10}$ adjusted p value. **(H)** Real-time PCR was conducted to measure relevant splicing change and total mRNA amount. Results are shown as percent spliced in (PSI) calculated as exon inclusion relative to total mRNA of the gene. Values represent averages of three RNA samples relative to two control samples ±SD [*p<0.05; **p<0.01; ***p<0.001]. **(I)** RNA was extracted from lymphoblasts of an FSHD2 patient and her healthy sister. Real-time PCR was conducted to measure the relevant splicing event and total mRNA amount. Results are shown as percent spliced in (PSI) calculated as exon inclusion relative to total mRNA of the gene. Values represent averages of three repeats [*p<0.05; **p<0.01; ***p<0.001].

two genes were both differentially expressed and alternatively spliced (Fig. 1F). As in FSHD2 patients, gene-set enrichment analysis for differentially spliced genes in the mNSC revealed a significant enrichment for phenotypes related to muscular dystrophy. 19% of mis-spliced genes (166 of 860 genes, FDR < 0.00018) are related to the “Abnormality of the musculoskeletal system” HPO (Fig. 1G).

To validate the splicing analysis, we chose ten leading candidate genes that were significantly mis-spliced and matched either a HPO annotation of "abnormal muscle physiology" or a GO annotation of "anatomical structure development". We performed qPCR on RNA from the same cells and found four of the ten genes to be significantly mis-spliced ($p < 0.05$, Student’s t-test) (Fig. 1H). One of the genes that presented a change in splicing has also demonstrated a change in total expression levels. To validate mis-splicing of the top five significant events in human we performed qPCR in FSHD2 patient lymphoblastoid cells (Supp. Fig. S1A-C), comparing to a healthy family member (Fig. 1I). All five events showed the expected change in splicing, and no significant change was detected in total expression levels (Supp. Fig. S1D).

To estimate the impact of Smchd1 on alternative splicing in other cell types, we also examined mouse embryonic fibroblasts (MEF). We reanalyzed available RNA-seq data from Smchd1^{MommeD1} homozygous mutant female MEFs[13] and found 3997 alternative splicing events in 2349 genes (rMATS, FDR < 5%, Supp. Fig. S1E). Gene-set enrichment analysis for differentially spliced genes in the MEFs revealed a significant enrichment for phenotypes related to muscular dystrophy (Supp. Fig. S1F). Together these findings indicate that Smchd1 regulates alternative splicing of hundreds of genes in mice. This regulation is cell-type specific, but Smchd1 is regulating a large subset of genes in both cell types (275 genes, $p < 0.00001$, Fisher’s exact test, Supp. Fig. S1G). Moreover, our results suggest that Smchd1 gene expression regulation is independent of its role in splicing regulation.

Smchd1 binding is enriched at mis-spliced exons

Next, we wanted to explore how Smchd1 regulates splicing. Since Smchd1 is a chromatin factor we wanted to explore the chromatin landscape at its splicing targets. We began by exploring whether Smchd1 directly binds mis-spliced exons. To this end we analyzed available Smchd1-GFP ChIP-seq data from neural stem cells of wildtype (WT) mice[11]. First, we assessed Smchd1 binding in the vicinity (5kb) of mis-spliced exons and compared to all exons expressed in either WT or Smchd1^{MommeD1} mNSC, regardless of whether they are mis-spliced or not. We found Smchd1 binds 169 (16%) of mis-spliced exons, compared to 11% of all expressed exons (Fig. 2A, $p < 0.0001$, Fisher’s exact test). Overall, Smchd1 binds mis-spliced exons 1.42 times

more often than all expressed exons. (Fig. 2A&B). Moreover, we compared Smchd1 binding in mis-spliced exons to other exons in the same genes that are not alternatively spliced and found Smchd1 binds the mis-spliced exons 1.41 times more often. (Fig. 2B).

Figure 2

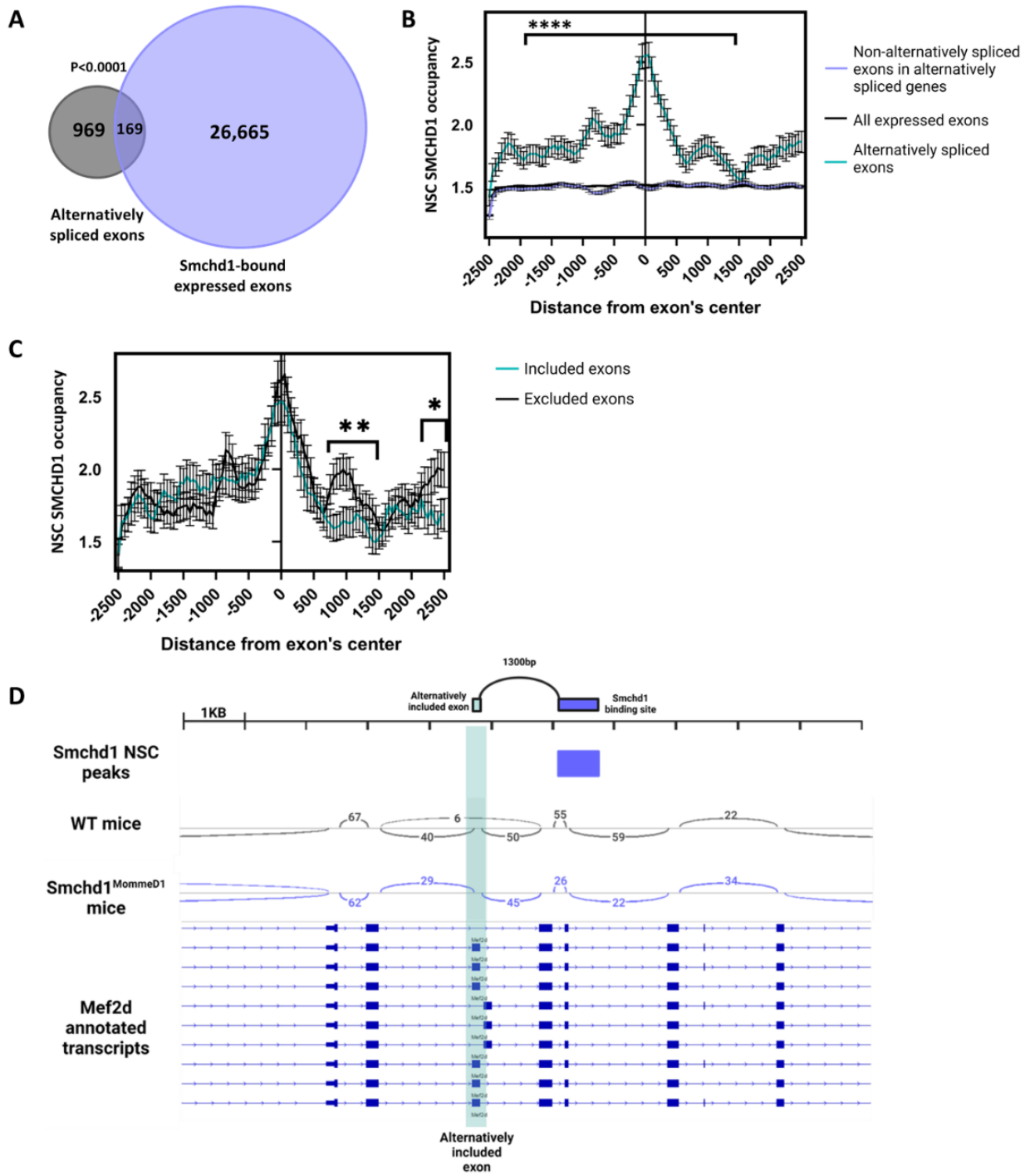

Figure 2: Smchd1 binding is enriched downstream of its regulated excluded exons. **(A-D)** Reanalysis of GFP ChIP-seq in primary NSCs with endogenous Smchd1-GFP fusion protein, analysis was limited to expressed genes only (TPM>1). **(A)** Venn diagram presenting the overlap of alternatively spliced exons and exons with nearby (<5kbp) Smchd1 binding site. **(B)** Aggregation plot depicting the average normalized Smchd1 occupancy, at and near exons alternatively spliced (turquoise), all expressed exons (black) or non-alternatively spliced exons (purple) in alternatively spliced genes, showing stronger binding of Smchd1 alternatively spliced exons [****p<0.0001]**.** X axis represent bins of size 50 bp around the center of the exon. **(C)** Aggregation plot depicting the average normalized Smchd1 occupancy at exons differentially included or excluded in Smchd1^{MommeD1} mice [*p<0.05, **<0.01]. X axis represent bins of size 50 bp around the center of the exon. **(D)** Genome browser view of the Mef2d alternatively spliced junctions presented by sashimi plots, arcs denote splice junctions quantified in spanning reads. Mutually exclusive alternatively spliced exon is highlighted in turquoise. Refseq transcripts are presented as a reference.

Interestingly, we found that Smchd1 preferentially binds downstream to exons that are included in Smchd1 null cells, but excluded when bound by Smchd1 in WT cells ("excluded exons") ($p < 0.01$, Wilcoxon test) (Fig. 2C). For example, exon 5 of Mef2d, a member of the myocyte-specific enhancer factor 2 (Mef2) family involved muscle cell differentiation and development[45]. Exon 5 is adjacent to an Smchd1 binding site and it is skipped in WT mice but included in Smchd1^{MommeD1} mice (Fig. 2D). We have repeated the analysis for another available NSC Smchd1-GFP ChIP-seq dataset [33] and found Smchd1 binds 1.38 more to mis-spliced exons compared to all expressed exons ($p < 0.00001$, Fisher's exact test) and specifically binds more to excluded exons ($p < 0.009$, student's t-test, Supp. Fig. S2A-C). Moreover, we repeated this analysis for MEFs, utilizing published Smchd1 binding data in MEF[13]. We observed a similar association with splicing: Mis-spliced exons had 16% more Smchd1 binding sites than all expressed exons ($p < 0.044$, Fisher's exact test), and Smchd1 binding preferentially binds downstream of excluded exons (Supp. Fig. S2D). Overall, our analysis demonstrates that binding of Smchd1 is enriched downstream of excluded exons, suggesting Smchd1 loss leads to aberrant inclusion of the exons.

Figure 3

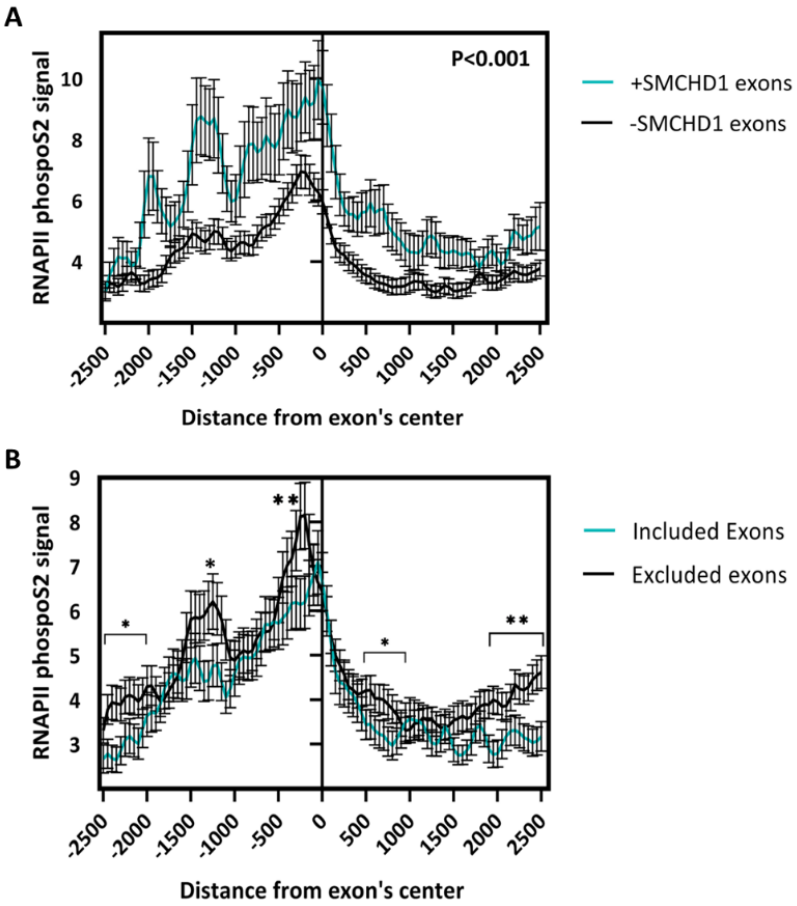

Figure 3: Smchd1 binding is associated with slow elongation rate of RNAPII. **(A-B)** Aggregation plots depicting the average normalized phospho-Ser2 levels of RNAPII at and near alternatively spliced exons differentially bound by Smchd1 **(A)** and at and near exons differentially included or excluded in Smchd1^{MommeD1} mice **(B)** in C2C12 cells. X axis represent bins of size 50 bp around the center of the exon [* FDR<0.05; ** FDR<0.01; *** FDR<0.001; ****p<0.0001].

Smchd1 binding correlates with RNAPII stalling at mis-spliced exons

Since RNAPII elongation rate can regulate alternative splicing we next asked whether Smchd1 binding is associated with RNAPII elongation. To address this, we reanalyzed ChIP-seq data of phosphoserine 2 of RNAPII carboxy terminal domain (pSer2), a marker of elongating RNAPII, from C2C12 mouse myoblasts [34]. Enrichment of pSer2 marks slow elongation rate or stalling of RNAPII [46]. We compared RNAPII pSer2 signal between mis-spliced exons with and without Smchd1 binding. Our analysis revealed a significant enrichment of RNAPII pSer2 in the exons bound by Smchd1 (Fig. 3A). We repeated the analysis for Smchd1 binding sites identified in a different NSC dataset[33] or in MEFs[13] and also found a significant enrichment of RNAPII pSer2 at Smchd1-bound mis-spliced exons (Supp. Fig. S3A-B). Moreover, we compared RNAPII pSer2 signal between included or excluded exons and found a specific enrichment at excluded exons (Fig. 3B). Together, these results suggest that Smchd1 binding in mis-spliced exons is correlated with RNAPII stalling and exon exclusion.

DNMT3B splicing is regulated by SMCHD1 in mice and human

Our analysis revealed that DNA methyltransferase 3 beta (DNMT3B) splicing is regulated by SMCHD1 in both human FSHD2 patient (Fig. 1I), mice NSCs (Fig. 1H, Supp. Fig.S4A) and MEFs (rMATS FDR < 0.0004). DNMT3B presented significant splicing changes in exons 5 and 21-22 in human, corresponding to exons 6 and 20-21 in mice. DNMT3B is known to have several alternatively spliced isoforms with distinct functions[38]. DNMT3B exon 21-22 encode part of the MTAse catalytic domain of the protein, but the function of the region encoded by exon 5 is unclear. Mutations of DNMT3B in FSHD are associated with D4Z4 hypomethylation and with high levels of DUX4 expression[20]. Specifically, a mutation in DNMT3B MTAse catalytic domain was shown to cause FSHD[20]. Alternative splicing of DNMT3B may affect D4Z4 methylation and thus contribute to the disease development. To validate SMCHD1 mediated alternative splicing of DNMT3B in human cells, we knocked down SMCHD1 by siRNA in HCT116 cells (Supp. Fig. S4B) and tested the inclusion of these exons. qPCR analysis showed a 60% increase in the inclusion of exon 5 ($p < 0.05$, student t-test) and two-fold increase in the inclusion of exon 21 ($p < 0.01$, student t-test) (Fig. 4A-B). Semi-quantitative PCR analysis showed a three-fold increase in exon 5 inclusion and 18-fold increase in exons 21-22 inclusion upon SMCHD1 knock-down (Fig. 4C-D, Supp. Fig. S4C-D). Overall, this demonstrates DNMT3B alternative splicing is indeed regulated by SMCHD1.

Our previous results suggested that SMCHD1 regulates alternative splicing by binding to the vicinity of the alternative exon and slowing RNAPII elongation rate. To test if DNMT3B

alternative splicing is mediated by slower RNAPII, we treated HCT116 cells with CPT, a topoisomerase inhibitor that slows RNAPII elongation. Our results show 70% reduction in total mRNA amount of DNMT3B and 35% reduction in exon 5 and 21 inclusion following treatment with CPT ($p < 0.01$, student t-test) (Fig. 4E-F and Supp. Fig. S4E), suggesting that RNAPII stalling indeed promotes exclusion of SMCHD1 regulated exons at DNMT3B gene.

Figure 4

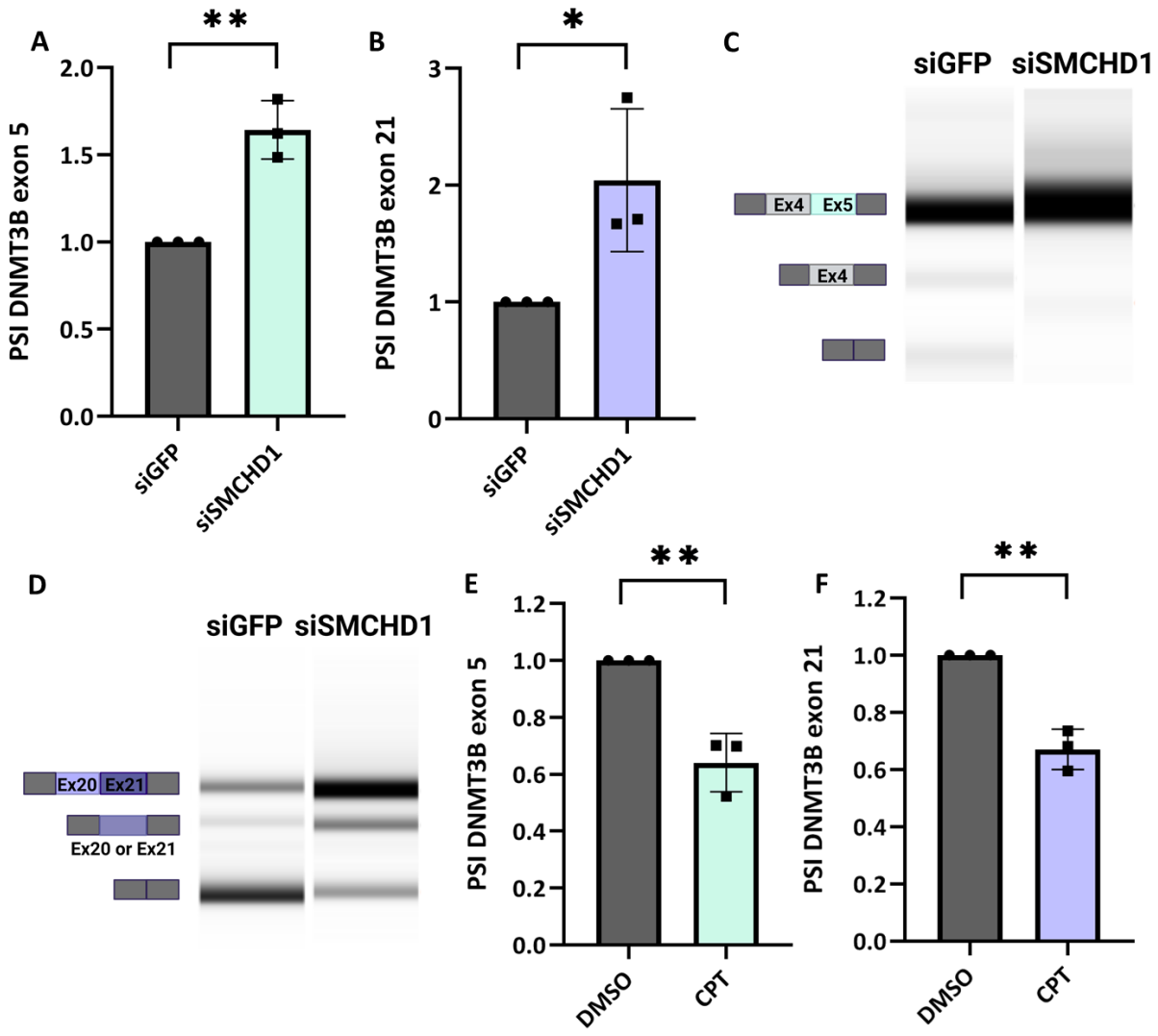

Figure 4: DNMT3B exon 5 and 21 are regulated by SMCHD1 and RNAPII stalling. **(A-D)** HCT116 cells were transfected with siRNA targeting SMCHD1 and GFP as negative control. Total RNA was extracted and analyzed by real-time PCR for DNMT3B exon 5 **(A)** and exon 21 **(B)** inclusion relative to DNMT3B total mRNA amount. PSI was calculated by dividing exon inclusion in DNMT3B total mRNA amount. Semi quantitative PCR was conducted for exons 4-5 **(C)** and exons 20-22 **(D)**. **(E-F)** HCT116 cells were treated with 6uM CPT or DMSO as negative control, for 6 hr. Total RNA was extracted and analyzed by real-time PCR for DNMT3B exon 5 **(E)** and exon 21 **(F)** inclusion relative to DNMT3B total mRNA amount. PSI was calculated by dividing exon inclusion in DNMT3B total mRNA amount. Values represent averages of three independent experiments ± SD; [* $p<0.05$; **$p<0.01$] (paired Student's t-test).

Identification of splicing factors regulating the alternative splicing of DNMT3B

Our previous findings suggest that SMCHD1 is promoting exon exclusion by RNAPII stalling. We hypothesize that RNAPII stalling by SMCHD1 promote exclusion by recruiting splicing factors. To predict which splicing factors may be involved we performed RNA binding proteins motif analysis on exons excluded by SMCHD1. To this end we compared excluded exons and their flanking 10 kb sequences to those of included exons in mice NSC and human FSHD2 patients. Our analysis found 35 significantly enriched motifs in human data and 17 in mice. Five motifs were found enriched in both datasets: RBFOX1, CPO, MSI, RBM5 and SRSF10 (Fig. 5A).

To experimentally identify potential splicing factors cooperating with SMCHD1, we performed an unbiased siRNA screen with the use of DNMT3B alternative splicing as readout. Specifically, we used a library of siRNA oligos directed to the 71 human splicing factors (as described in SpliceAid-F[47]) in HCT116 cells. We monitored alternative splicing of DNMT3B exons 5 and 21 using qPCR. As SMCHD1 is regulating the alternative splicing of both exon 5 and 21 of DNMT3B, we expected that a splicing factor working with SMCHD1 will regulate both events. Z scores was calculated for the average PSI of exons 5 or 21 separately. Splicing factors for which both z scores are higher than the positive control (siSMCHD1), and for which the sum of both z scores was higher than 2 were considered for downstream analysis. The screen identified seven factors: RBM5, SYNCRIP, HNRNPH2, NOVA2, PTBP2, ELAVL3, ELAVL1 (Fig. 5B). Of those seven factors we filtered out factors with expression level below detection rate and eventually found five hits: RBM5, SYNCRIP, HNRNPH2, NOVA2 and PTBP2 (Supp. Fig. S4F). To validate these hits, we conducted a secondary screen knocking down each splicing factor by siRNA in HCT116 cells and tested the inclusion of DNMT3B exons, while monitoring the knock-down level of each splicing factor (Supp. Fig. S4G). qPCR analysis showed a significant increase in the inclusion of DNMT3B exons only for RBM5 ($p<0.017$, student t-test) (Fig. 5C). Overall, motif enrichment and splicing factor screen suggest RBM5 as a potential ally of SMCHD1 in its alternative splicing regulation.

DNMT3B alternative splicing is regulated by SMCHD1 via RBM5

We hypothesis that SMCHD1 binding to the DNA stall RNAPII to allow for RBM5 binding to pre-mRNA. To check our hypothesis, we silenced SMCHD1 and measured the binding of RBM5 using RNA-IP to DNMT3B pre-mRNA. To this end we performed RNA-IP for RBM5 in HCT116 cells. Monitoring DNMT3B introns 4 and 21 relative to input, we found silencing of SMCHD1 led to a reduction of 50% and 70% in RBM5 binding, respectively ($p<0.013$ and $p<0.017$,

Figure 5

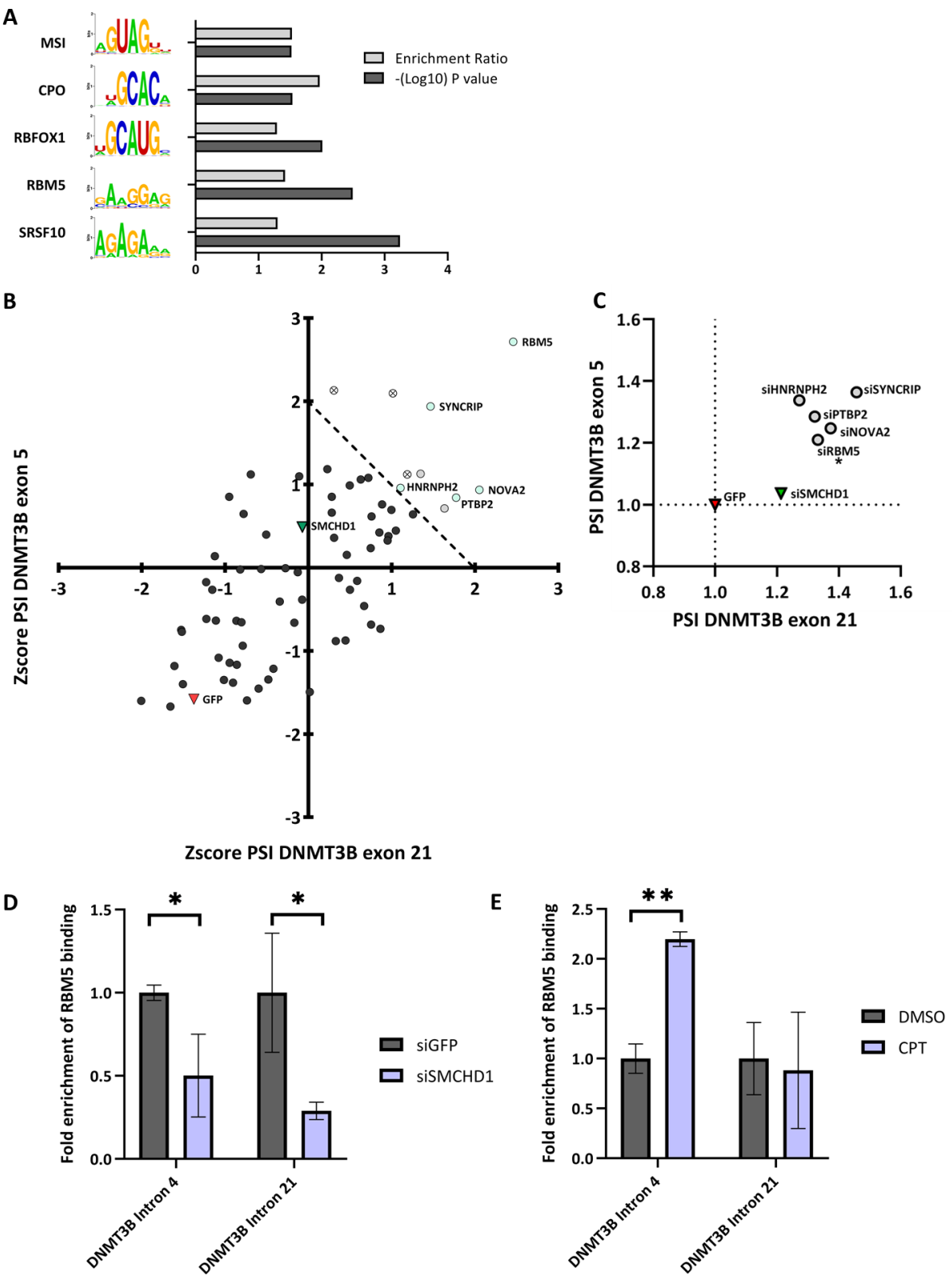

Figure 5: DNMT3B exon 5 and 21 are regulated by RBM5. **(A)** Enrichment of binding sites of SMCHD1 regulated exons: Enriched RNA motifs in alternatively excluded exons in both mice and human compared to included exons. **(B)** HCT116 cells were transfected with siRNA targeting 71 human splicing factor, SMCHD1 as a positive control and GFP as negative control. Total RNA was extracted and analyzed by real-time PCR for DNMT3B exon 5 and exon 21. Z scores were calculated for DNMT3B exon 5 and exon 21 PSI, as DNMT3B exon inclusion/DNMT3B total mRNA and normalized to siGFP as a negative control. Shown in scatter plot: red triangle represent GFP (negative control) , green triangle represent SMCHD1 (positive control), gray circles represent hits with low expression, crossed circles represent hits high variance between repeats and blue circles represent splicing factor hits. **(C)** HCT116 cells were transfected with siRNA targeting the splicing factor hits and GFP as a negative control. Total RNA was extracted and analyzed by real-time PCR for DNMT3B exon 5 and exon 21 inclusion relative to DNMT3B total mRNA amount. PSI was calculated as DNMT3B exon inclusion/DNMT3B total mRNA and normalized to negative control. Values represent averages of three repeats ±SD. Negative control (siGFP) PSI is represented by the dotted line at 1; [* p<0.05] (Student's t-test). **(D)** RNA-Immunoprecipitation of RBM5 in HCT116 transfected with siSMCHD1 or negative control (siGFP) for 72 h. Real-time PCR for DNMT3B intron 4 and 21 relative to input. **E.** HCT116 cells were treated with 6uM CPT or DMSO as negative control, for 6 hr. Real-time PCR for DNMT3B intron 4 and 21 relative to input. (D-E) Values represent averages of three technical replicates ±SD; [* p<0.05,** p<0.01] (paired Student's t-test).

student t-test) (Fig. 5D). This result suggests that SMCHD1 is a regulator of RBM5 binding to DNMT3B's pre-mRNA.

To test whether RNAPII stalling mediate RBM5 binding we performed RNA-IP following CPT treatment and found a 2-fold increase in RBM5 binding to DNMT3B intron 4 ($p<0.004$, student t-test) while there was no change in RBM5 binding to DNMT3B intron 21 (Fig. 5E). Overall, these results support the hypothesis that the RBM5 and SMCHD1 proteins functionally interact in the regulation of DNMT3B alternative splicing and that RBM5 recruitment to DNMT3B exon 5 is affected by RNAPII stalling.

Figure 6

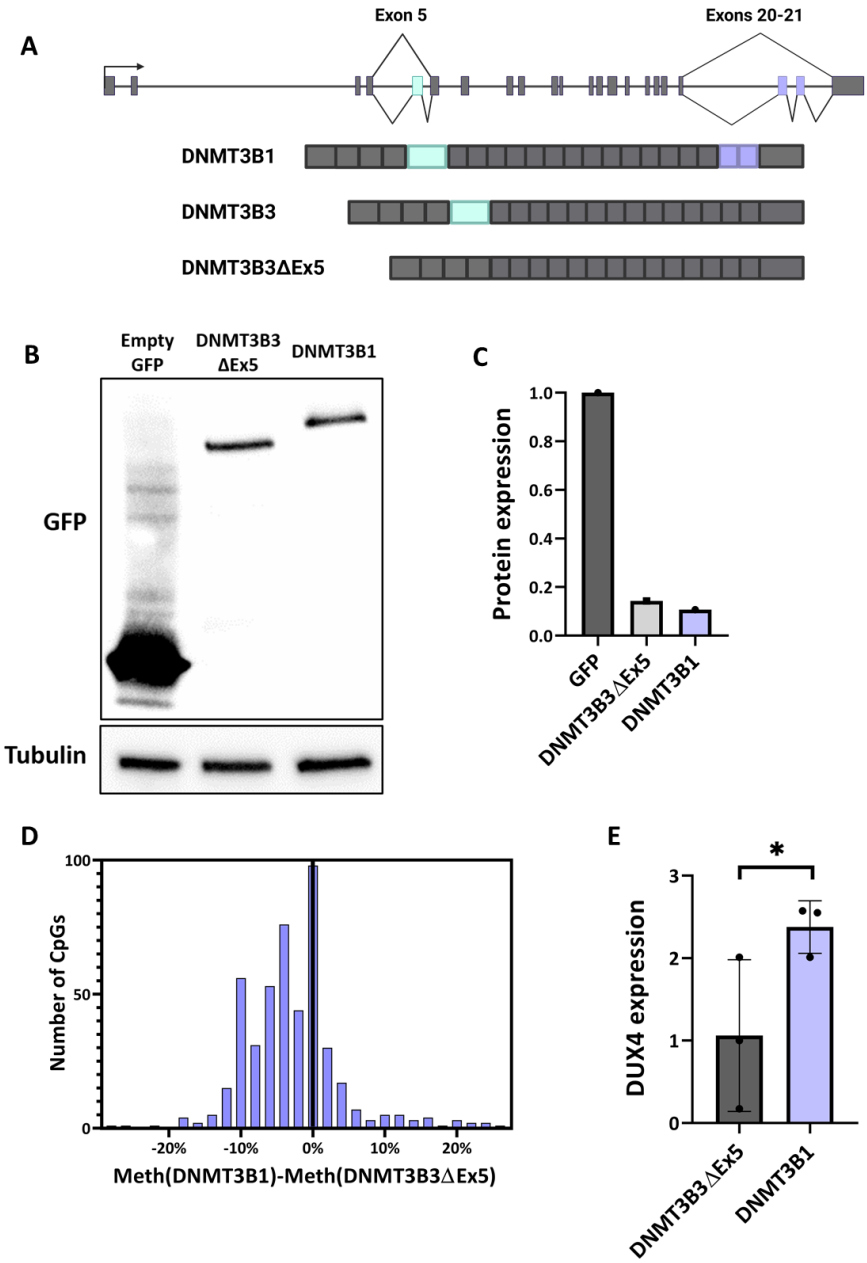

Figure 6: DNMT3B1 isoform reduces methylation at the D4Z4 region leading to increase of DUX4 expression. **(A)** Schematic representation of the *DNMT3B* gene and its alternatively spliced isoforms. **(B-C)** DNMT3B null HCT116 cells were infected with lentiviruses containing empty-GFP, GFP-DNMT3B3ΔEx5 or GFP-DNMT3B1. Western blot conducted with the indicated antibodies **(B)** shows successful infection. Bands were quantified and normalized to Tubulin (**C**). **(D)** DNA was isolated from cells with each of the isoforms and converted with bisulfite. PCR products of three locations along the D4Z4 region were sequenced, and methylation levels in each CpG were assessed using Biscuit. Histogram presents difference in methylation level measured over 470 CpGs in the D4Z4 region. **(E)** RNA was extracted from cells with the DNMT3B3ΔEx5 and DNMT3B1 isoforms and real-time PCR was conducted. DUX4 mRNA level was quantified relative to *CycloA* reference gene. Values represent averages of three technical replicates ±SD; [* $p<0.05$] (Student's t-test).

DNMT3B alternative splicing promotes D4Z4 hypomethylation and DUX4 expression

SMCHD1 mutations promote aberrant inclusion of both exons 5 and 20-21 of DNMT3B, and DNMT3B mutations were previously associated with DUX4 expression and D4Z4 hypomethylation[20]. Thus, we next aimed to test whether DNMT3B isoforms cause hypomethylation of D4Z4 region and promote DUX4 expression. To test the impact of each DNMT3B isoform on D4Z4 methylation, we infected DNMT3B-null HCT116 cells with either GFP-DNMT3B1, GFP-DNMT3B3ΔEx5 or an empty GFP vector (Fig. 6A-C, Supp. Fig. S5). Stable cell lines were grown for 14 days to allow robust accumulation of DNA methylation. We determined DNA methylation levels at three regions of D4Z4 array using bisulfite-PCR sequencing, and found a significant decrease in D4Z4 methylation in DNMT3B1 expressing cells compared to DNMT3B3ΔEx5 cells ($p < 0.00001$, student's t-test) (Fig. 6D). Interestingly, DNMT3B1 cells presented decreased methylation level in several regions compared to cells infected with empty GFP vector, and therefore no active DNMT3B at all ($p < 0.02$, student's t-test) (Supp. Fig. S5). Overall, these results show that DNMT3B alternatively spliced isoforms differentially regulate DNA methylation, and specifically at the D4Z4 locus. Next, we assessed the expression level of DUX4 mRNA in these cell lines by qPCR[48] and found a 2-fold increase in DUX4 expression in DNMT3B1 expressing cells ($p < 0.04$, student t-test) (Fig. 6E). Together with our finding that SMCHD1 mutations shift DNMT3B splicing towards the DNMT3B1 isoform, this suggest that SMCHD1 mutations drive FSHD2 pathogenesis by altering DNMT3B splicing and prompting D4Z4 hypomethylation and DUX4 expression.

Discussion

In this work, we identify a novel role for SMCHD1 as a splicing regulator and suggest a mechanism for its action. While SMCHD1 is known to regulate chromosomal interactions and gene expression, here we show for the first time that it is also a splicing regulator. While previous reports did not detect differential isoform usage in Smchd1^{MommeD127}, here we profiled mRNA by very deep sequencing accompanied by detailed differential spicing analysis allowing a more robust detection of exon inclusion and exclusion events. We suggest a mechanism in which SMCHD1 binding modulates RNAPII elongation rate. We hypothesize that RNAPII stalling is allowing the recruitment of inhibitory splicing factors and identify RBM5 as a potential ally in SMCHD1 regulatory pathway (Fig. 7).

Several chromatin modulators have previously been shown to act as regulators of splicing, and different mechanisms for chromatin-mediated splicing regulation have been identified. Our results suggest that SMCHD1 regulation of splicing is mediated by RNAPII kinetics, similar to the mechanism suggested for CTCF mediated splicing regulation[6,7]. While CTCF is slowing RNAPII to promote exon inclusion, we have found that SMCHD1-mediated slow RNAPII kinetics is correlating with exon exclusion (Fig. 3B) and is mediated by recruitment of splicing factors and specifically RBM5 (Fig. 5A-D). Specifically, we show that SMCHD1 binds the vicinity of its target exons to stall RNAPII and allow for RBM5 binding to pre-mRNA (Fig. 2B). Overall, our results reveal a new mechanism for chromatin-mediated splicing regulation.

Figure 7

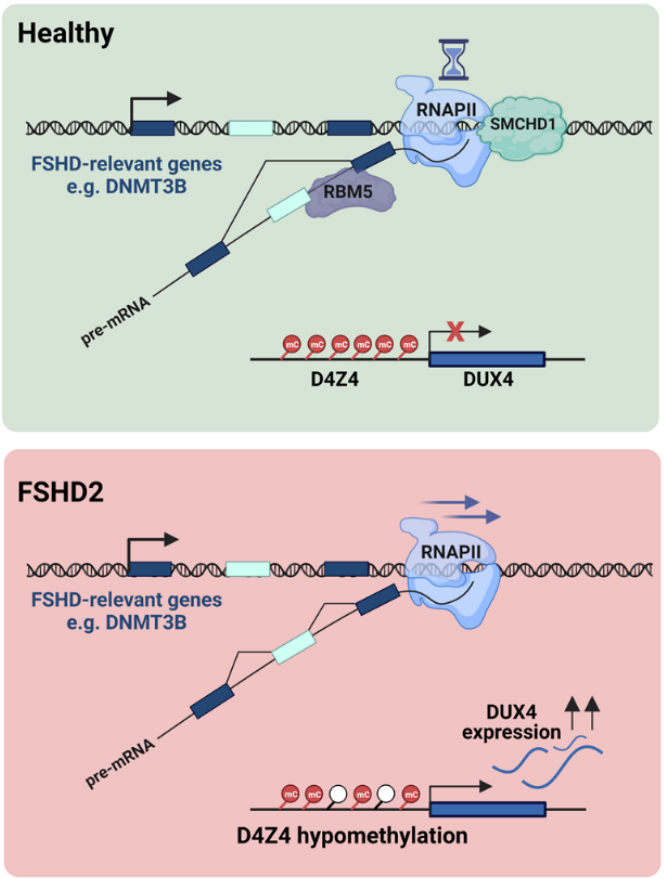

Figure 7: Model for SMCHD1 pathophysiology in FSHD2 driven by its abnormal splicing. In healthy cells, SMCHD1 binding is specifically enriched in the proximity of alternative exons, particularly excluded exons. A slower rate of RNAPII elongation is linked to SMCHD1 binding and related to exon exclusion. Excluded exons are characterized by a high density of RBM5 motifs, which inhibit exon inclusion and promote exon exclusion. However, in FSHD2 muscle cells, SMCHD1 mutations lead to abnormal exon inclusion. This mis-splicing of FSHD-related genes, including DNMT3B, results in decreased methylation of the D4Z4 region and increased expression of the DUX4 gene.

We found SMCHD1 to regulate the splicing of multiple genes with a potential clinical significance for FSHD2 development. We have found aberrant splicing of hundreds of genes that are known as key factors for myocyte function and mutations in dozens of them have

been previously identified as pathogenic in muscular dystrophy. For example, Titin (TTN) is mis-spliced in FSHD2 patients. Mutations in TTN are a known cause for several muscular dystrophies[49], including limb-girdle muscular dystrophy (LGMD), and has many alternatively spliced isoforms with distinct functions[50], suggesting that splicing alteration of this gene can be associated with muscular pathology. Another example is the *calpain 3 (CAPN3)* gene which is mis-spliced in FSHD2 patients and its mutations are causing LGMD as well[51]. *CAPN3* have been previously identified as significantly alternatively spliced in FSHD1 patients and its alternative splicing resulted in muscle cells differentiation defect [52], suggesting it has different functioning isoforms. We have found that *CAPN3* is also differentially spliced between FSHD1 and FSHD2 patients, at different exons from the previously reported one in FSHD1. Specifically, the splicing alteration we have identified in exons 15-16 was previously described to disrupt skeletal muscle mass[53]. Moreover, we found significant alternative splicing changes in *Troponin T 1 (TNNT1)* and *TNNT3* genes in FSHD2 patients. Both genes are key factors in myocyte function and have known alternatively spliced isoforms[54].TNNT3 has been previously shown as alternatively spliced in FSHD and its aberrant splicing was found to characterizes dystrophic muscles in FSHD patients[55,56] Overall, the cumulative effect these alterations and others we have identified may contribute to the phenotype of FSHD.

In this work we focus on SMCHD1 prominent target, DNMT3B, which is mutated in FSHD4 patients. Previous findings indicate Dnmt3b is binding to the D4Z4 array and its knockdown results in elevated DUX4 expression[57]. While SMCHD1 mutations are known to be present in FSHD2 patients and are associated with D4Z4 hypomethylation and DUX4 expression, the specific mechanism for SMCHD1-associated hypomethylation is unclear. Our findings suggest that mutations in SMCHD1 lead to mis-splicing of multiple genes including DNMT3B, supporting the DNMT3B1 isoform over the DNMT3B3 isoform (Fig. 1I). Finally, DNMT3B mis-splicing cause aberrant DNA methylation, including at D4Z4 which causes an increase in DUX4 expression leading to FSHD2 development (Fig. 6D-E, 7). Our results suggest a novel mechanism for FSHD pathogenesis orchestrated by SMCHD1 (Fig. 7).

In our work we present that the aberrant expression of DNMT3B1 isoform, which is the only isoform containing the MTAse domain and is 'active', is associated with D4Z4 hypomethylation. While the known role of the isoform is opposing the observed finding[58], we hypothesis that DNMT3B active-inactive isoform balance is important for the methylation regulated by DNMT3B-DNMT3A-DNMT3L complex. DNMT3B inactive isoforms have been previously shown to enhance DNA methylation and have been suggested as accessory proteins to recruit and positively regulate DNMT3A[59,60]. Specifically, previous studies indicate

a gain in Dnmt3a catalytic efficiency following the presence of Dnmt3b inactive isoforms and that Dnmt3a and Dnmt3b3 form a stable complex[60]. Moreover, reintroduction of DNMT3B inactive isoforms constructs in DNMT3B null cells was shown to cause genome-wide methylation restoration in a similar matter to that of DNMT3B1 active isoform[59]. Thus, it may be possible that the absence of the inactive isoform, that play as a crucial co-factor of DNMT3 complex activity, leads to hypomethylation. Thus, mis-splicing and down regulation of the inactive isoform may disrupt methylation of D4Z4 and cause FSHD.

Methods

Cell lines

HCT116 (ATCC Number: CCL-247) cells were grown in Dulbecco's modified Eagle's medium (DMEM) supplemented with 10% fetal bovine serum. Lymphoblastoid cell lines were grown in RPMI-1640 supplemented with 20% fetal bovine serum. Cell lines were maintained at 37°C and 5% CO_2 atmosphere.

Ethics Statement

Human samples were obtained from under the Hadassah Institutional Helsinki committee, approval no. 0198-11 HMO. All patients gave written informed consent.

RNA sequencing and analysis

RNA from WT and Smchd1-null (Smchd1$^{MommeD1/MommeD1}$) NSCs from embryonic day 14.5 (E14.5) mouse brains was obtained as previously described[27]. We performed next-generation sequencing, using RNA ScreenTape kit (catalog #5067-5576; Agilent Technologies), D1000 ScreenTape kit (catalog #5067-5582; Agilent Technologies), Qubit RNA HS Assay kit (catalog # Q32852; Invitrogen), and Qubit DNA HS Assay kit (catalog #32854; Invitrogen) were used for each specific step for quality control and quantity determination of RNA and library preparation. For mRNA library preparation: TruSeq RNA Library Prep Kit v2 was used (Illumina). In brief, 1 µg was used for the library construction; library was eluted in 20 µL of elution buffer. Libraries were adjusted to 10 mM, and then 10 µL (50%) from each sample was collected and pooled in one tube. Multiplex sample pool (1.5 pM including PhiX 1.5%) was loaded in NextSeq 500/550 High Output v2 kit (75 cycles cartridge and 150 cycles cartridge; Illumina). Run conditions were in paired end (43 × 43 bp and 80 × 80 bp, respectively) and loaded on NextSeq 500 System machine (Illumina). mNSC RNA-seq data have been deposited in NCBI's Gene Expression Omnibus and are accessible through GEO Series accession number

GSE223039. FSHD patients' RNA-seq data was obtained from the GEO database, accession GSE56787[18]. SMCHD1 mutant MEF RNA-seq data was obtained from GEO, accession GSE121184[13].

Reads were aligned to the mm10 (mNSC and MEF) or hg38 (FSHD patients) using STAR version 2.7.10[28] with default parameters. We counted reads in genes with featureCounts version 2.0.1[29] using GENCODE release M21 (mNSCs and MEFs) or GENCODE release 33 (FSHD patients). DESeq2[30] was used to identify differentially expressed genes. rMATS (version 4.1.1)[31] was used to identify differential alternative splicing events. For each alternative splicing event, we used the calculation on both the reads mapped to the splice junctions and the reads mapped to the exon body (JCEC). Gene-set enrichment analysis was performed using g:Profiler[32]. To limit bias due to inability to call differential splicing in lowly expressed genes, we limited the analysis only to genes with expression > 1 TPM, comparing alternatively spliced genes with > 1 TPM to all genes with > 1 TPM. False discovery rate (FDR) was controlled by the Benjamini-Hochberg procedure.

ChIP sequencing and analysis

Smchd1-GFP NSC ChIP-seq data was obtained from the GEO database, accession GSE111722[11] and GSE174066[33]. Smchd1 MEF ChIP-seq data was obtained from the GEO database, accession GSE111820[13]. RNAPII phospoS2 in C2C12 cells was obtained from ENCODE[34], accession ENCSR000AIU. For Smchd1 ChIP, FASTQ files were obtained using SRA-toolkit (version 3.0.0) and aligned to mm10 genome with BWA-mem (version 0.7.17)[35] using default parameters. PCR duplicates were marked and removed using Samtools (version 1.15.1)[36]. Peak calling and annotation were performed using HOMER version 4.11[37]. Peak calling was done for Smchd1 peaks using the 'histone' mode, otherwise default parameters were used. Peak calling was done relative to background signal, using input for Smchd1-MEF data, whole cell extract for Smchd1-GFP NSC data (2021 dataset, GSE174066) and GFP ChIP-seq in WT cells for Smchd1-GFP NSC data (2018 dataset, GSE111722). ChIP signal estimation and visualization was done using HOMER annotatePeaks tool histogram mode, with the following parameters: -size 5000 -hist 50 -ghist. Average ChIP signal and SEM was calculated for each 50bp genomic bin. Significance of differential binding was called using Wilcoxon test with FDR correction by the Benjamini-Hochberg procedure.

siRNA interference

Human HCT116 cells were seeded in 6-well culture plates (1.75 x 10^5 cells/well). After 24 hours, cells were transfected with 20 µM of esiRNA (Sigma). using TransITx2 system Mirus

Bio™ (MIR2700, Thermo Fisher Scientific) following manufacturer's instructions. As a control, cells were transfected with esiRNA directed for GFP (EHUEGFP, Sigma). For each condition cells were seeded as triplicates and collected for examination after 72 hours.

CPT treatment

To impede the dynamics of transcribing RNAPII, HCT116 cells were plated to achieve 60% confluency and treated with camptothecin (CPT, Sigma) to a final concentration of 6 µM for 6 h. As a control, cells were treated with DMSO at the same concentration.

qRT-PCR

RNA was isolated using the GENEzol™ TriRNA Pure Kit (Geneaid). With the qScript cDNA Synthesis Kit (Quantabio), cDNA was synthesized from 1 µg RNA in a 20-µl reaction volume and afterwards diluted to 4 ng/µl. For quantitative real-time PCR 20 ng cDNA and 1 pmol/µl primers were mixed with 2x SYBR (BioRad) in a total volume of 13 µl for each well. Cyclophilin A was used as a reference gene. Reactions were performed for 40 cycles with a T_m of 60 °C. Primers used in this study are provided in Supplementary Table S1.

siRNA splicing factor screen

EsiRNA library targeting 71 human splicing factors was purchased from sigma. HCT116 cells were seeded in 96-well plate and reverse transfected with 50 nM of esiRNA using Mirus TransITx2 system. We used siSMCHD1 as positive control and siGFP (Sigma) as negative control. After 72 hours, cells were lysed with BioRad's SingleShot buffer. Cell lysate was used directly for cDNA synthesis followed by qPCR.

Lymphoblastoid cell line establishment

Venous blood was collected in EDTA coated tubes. PBMC separation was performed using Lymphoprep (Stemcell Technologies). Cells were incubated with B95 cell line media containing EBV and Cyclosporine was added for seven days' incubation.

RNA Immunoprecipitation

Cells were washed with ice-cold PBS, harvested, and lysed for 30 min on ice in a buffer containing 0.5% NP-40 150 mM NaCl, 50 mM Tris-HCl pH = 7.5, and 1 mM EDTA supplemented with protease and RNasin inhibitors followed by sonication in an ultrasonic bath (Qsonica, Q800R2 Sonicator) for six cycles of 5 sec ON and 30 sec OFF. Supernatants were collected after centrifugation at 16,000g for 20 min. Antibody with beads were incubated for 2h at 4°C. Sonicated lysate with pre-incubated beads were added for an additional 4h. Beads were washed four times and GeneZol added for RNA extraction. Serial dilutions of the 10% input

cDNA (1:2, 1:10, 1:50, 1:250) were analyzed by real-time qPCR. The oligonucleotide sequences used are listed in Supplemental Table S1.

Stable cell line establishment

pLenti CMV GFP Puro (Addgene, plasmid #17448) plasmid was cut with BsrgI and SalI restriction enzymes. Sequences of DNMT3B transcripts were isolated from pcDNA4-DNMT3B1 and pcDNA4-DNMT3B3ΔEx5 plasmids[38] by PCR and assembled with pLenti construct using Gibson assembly (New England Biolabs) following the manufacturer protocol.

Lentiviruses were produced by transfection in the HEK293T packaging cell-line using PEI transfection reagent. Cells were transfected with each DNMT3B or GFP-only constructs in addition to pCMV-dR8.2 dvpr (Addgene, plasmid #8455) and pCMV VSV-G (Addgene, plasmid #8454) lentiviral particles.

DNMT3B-null HCT116 cells[39] were infected with viral particles and selected with Puromycin. Cells were incubated for 14 days to allow for stable expression and methylation dynamics.

Bisulfite sequencing and analysis

Bisulfite conversion was performed using Zymo MethylGold kit following the manufacturer protocol. PCR reaction to isolate D4Z4 region was done by using four previously described primer sets[40] containing Illumina adaptor sequences at both the 5' and 3' ends. PCR reaction was done with Taq Mix Red PCR MasterMix (Tamar). PCR products were cleaned and directly amplified using primers for the Illumina adaptor sequences followed by DNA sequencing. Methylation analysis was done using Biscuit (version 1.0.2). Reads were aligned using Biscuit align to GRCh38 genome. Methylation level was estimated using Biscuit pileup with the following parameters: -b 0 -m 0 -a 0 -l 1 -5 1 -3 1 -c -n 1000 -d -u -p -o, followed by biscuit vcf2bed tool with -t cg parameter. Otherwise, default parameters were used.

Motif enrichment analysis

RNA-binding protein motif enrichment was performed using the SEA tool from the MEME suite (version 5.5.0)[41]. Enrichment analysis was performed for excluded exons sequences with included exons sequences as background, for human FSHD and mouse NSC results separately. FASTA files were generated using BEDTools getfasta tool (version 2.30.0)[42] with hg38 and mm10 reference genomes, respectively. SEA analysis was performed using default parameters and default E-value of ≤ 10, using the motif database: Ray2013 RNA (DNA-encoded)[43].

Acknowledgements

We thank Marnie Blewitt for valuable advice and Smchd1^{MommeD1} NSC RNA. We thank Abed Nasereddin and Idit Shiff from the Genomic Applications Laboratory, The Core Research Facility, The Faculty of Medicine - Ein Kerem, The Hebrew University of Jerusalem, Israel, for their professional advice and RNA-seq service. We thank Amos Tanay for DNMT3B-KO HCT116 cells. We thank Keith Robertson for pcDNA4-DNMT3B1, pcDNA4-DNMT3B3ΔEx5 plasmids. This work was supported by the Concern Foundation and AFHU / Boehm Foundation Young Professorship Award and the Alon Fellowship (YD).

References

1. Griffin, C. & Saint-Jeannet, J.-P. Spliceosomopathies: Diseases and mechanisms. *Dev. Dyn.* **249**, 1038–1046 (2020).
2. Yoshida, K. & Ogawa, S. Splicing factor mutations and cancer. *Wiley Interdiscip. Rev. RNA* **5**, 445–459 (2014).
3. Naftelberg, S., Schor, I. E., Ast, G. & Kornblihtt, A. R. Regulation of Alternative Splicing Through Coupling with Transcription and Chromatin Structure. *Annu. Rev. Biochem.* **84**, (2015).
4. Cramer, P., Pesce, C. G., Baralle, F. E. & Kornblihtt, A. R. Functional association between promoter structure and transcript alternative splicing. *Proc. Natl. Acad. Sci.* **94**, 11456–11460 (1997).
5. Dujardin, G. *et al.* How Slow RNA Polymerase II Elongation Favors Alternative Exon Skipping. *Mol. Cell* **54**, 683–690 (2014).
6. Ruiz-Velasco, M. *et al.* CTCF-Mediated Chromatin Loops between Promoter and Gene Body Regulate Alternative Splicing across Individuals. *Cell Syst.* **5**, 628-637.e6 (2017).
7. Alharbi, A. B., Schmitz, U., Bailey, C. G. & Rasko, J. E. J. CTCF as a regulator of alternative splicing: new tricks for an old player. *Nucleic Acids Res.* **49**, 7825–7838 (2021).
8. Salton, M., Voss, T. C. & Misteli, T. Identification by high-throughput imaging of the histone methyltransferase EHMT2 as an epigenetic regulator of VEGFA alternative splicing. *Nucleic Acids Res.* **42**, 13662–13673 (2014).
9. Siam, A. *et al.* Regulation of alternative splicing by p300-mediated acetylation of splicing factors. *RNA* **25**, 813–824 (2019).
10. Blewitt, M. E. *et al.* SmcHD1, containing a structural-maintenance-of-chromosomes hinge domain, has a critical role in X inactivation. *Nat. Genet.* **40**, (2008).
11. Jansz, N. *et al.* Smchd1 regulates long-range chromatin interactions on the inactive X chromosome and at Hox clusters. *Nat. Struct. Mol. Biol.* **25**, 766–777 (2018).

12. Chen, K. *et al.* Genome-wide binding and mechanistic analyses of Smchd1-mediated epigenetic regulation. *Proc. Natl. Acad. Sci.* **112**, (2015).
13. Gdula, M. R. *et al.* The non-canonical SMC protein SmcHD1 antagonises TAD formation and compartmentalisation on the inactive X chromosome. *Nat. Commun.* **10**, 30 (2019).
14. Brideau, N. J. *et al.* Independent Mechanisms Target SMCHD1 to Trimethylated Histone H3 Lysine 9-Modified Chromatin and the Inactive X Chromosome. *Mol. Cell. Biol.* **35**, 4053–4068 (2015).
15. Wang, C.-Y., Jégu, T., Chu, H.-P., Oh, H. J. & Lee, J. T. SMCHD1 Merges Chromosome Compartments and Assists Formation of Super-Structures on the Inactive X. *Cell* **174**, 406-421.e25 (2018).
16. Chen, K. *et al.* The epigenetic regulator Smchd1 contains a functional GHKL-type ATPase domain. *Biochem. J.* **473**, 1733–1744 (2016).
17. Larsen, M. *et al.* Diagnostic approach for FSHD revisited: SMCHD1 mutations cause FSHD2 and act as modifiers of disease severity in FSHD1. *Eur. J. Hum. Genet.* **23**, (2015).
18. Yao, Z. *et al.* DUX4-induced gene expression is the major molecular signature in FSHD skeletal muscle. *Hum. Mol. Genet.* **23**, 5342–5352 (2014).
19. Deutekom, J. C. T. V. *et al.* FSHD associated DNA rearrangements are due to deletions of integral copies of a 3.2 kb tandemly repeated unit. *Hum. Mol. Genet.* **2**, 2037–2042 (1993).
20. Boogaard, M. L. van den *et al.* Mutations in DNMT3B Modify Epigenetic Repression of the D4Z4 Repeat and the Penetrance of Facioscapulohumeral Dystrophy. *Am. J. Hum. Genet.* **98**, 1020–1029 (2016).
21. Hamanaka, K. *et al.* Homozygous nonsense variant in *LRIF1* associated with facioscapulohumeral muscular dystrophy. *Neurology* **94**, e2441–e2447 (2020).
22. Sacconi, S. *et al.* The FSHD2 gene SMCHD1 is a modifier of disease severity in families affected by FSHD1. *Am. J. Hum. Genet.* **93**, 744–751 (2013).

23. Sacconi, S. *et al.* FSHD1 and FSHD2 form a disease continuum. *Neurology* **92**, e2273–e2285 (2019).
24. Shaw, N. D. *et al.* SMCHD1 mutations associated with a rare muscular dystrophy can also cause isolated arhinia and Bosma arhinia microphthalmia syndrome. *Nat. Genet.* **49**, (2017).
25. Gordon, C. T. *et al.* De novo mutations in SMCHD1 cause Bosma arhinia microphthalmia syndrome and abrogate nasal development. *Nat. Genet.* **49**, (2017).
26. Mul, K. *et al.* FSHD type 2 and Bosma arhinia microphthalmia syndrome. *Neurology* **91**, (2018).
27. Dong, X. *et al.* The long and the short of it: unlocking nanopore long-read RNA sequencing data with short-read differential expression analysis tools. *NAR Genomics Bioinforma.* **3**, lqab028 (2021).
28. Dobin, A. *et al.* STAR: ultrafast universal RNA-seq aligner. *Bioinformatics* **29**, 15–21 (2013).
29. Liao, Y., Smyth, G. K. & Shi, W. featureCounts: an efficient general purpose program for assigning sequence reads to genomic features. *Bioinformatics* **30**, 923–930 (2014).
30. Love, M. I., Huber, W. & Anders, S. Moderated estimation of fold change and dispersion for RNA-seq data with DESeq2. *Genome Biol.* **15**, 550 (2014).
31. Shen, S. *et al.* rMATS: Robust and flexible detection of differential alternative splicing from replicate RNA-Seq data. *Proc. Natl. Acad. Sci.* **111**, (2014).
32. Raudvere, U. *et al.* g:Profiler: a web server for functional enrichment analysis and conversions of gene lists (2019 update). *Nucleic Acids Res.* **47**, W191–W198 (2019).
33. Tapia del Fierro, A. *et al. SMCHD1 has separable roles in chromatin architecture and gene silencing that could be targeted in disease*. http://biorxiv.org/lookup/doi/10.1101/2021.05.12.443934 (2021) doi:10.1101/2021.05.12.443934.

34. Yue, F. *et al.* A comparative encyclopedia of DNA elements in the mouse genome. *Nature* **515**, 355–364 (2014).

35. Li, H. & Durbin, R. Fast and accurate short read alignment with Burrows-Wheeler transform. *Bioinformatics* **25**, 1754–1760 (2009).

36. Danecek, P. *et al.* Twelve years of SAMtools and BCFtools. *GigaScience* **10**, giab008 (2021).

37. Heinz, S. *et al.* Simple combinations of lineage-determining transcription factors prime cis-regulatory elements required for macrophage and B cell identities. *Mol. Cell* **38**, 576–89 (2010).

38. Gopalakrishnan, S. *et al.* A Novel DNMT3B Splice Variant Expressed in Tumor and Pluripotent Cells Modulates Genomic DNA Methylation Patterns and Displays Altered DNA Binding. *Mol. Cancer Res.* **7**, 1622–1634 (2009).

39. Rhee, I. *et al.* DNMT1 and DNMT3b cooperate to silence genes in human cancer cells. *Nature* **416**, 552–556 (2002).

40. Dion, C. *et al.* SMCHD1 is involved in *de novo* methylation of the *DUX4* -encoding D4Z4 macrosatellite. *Nucleic Acids Res.* **47**, 2822–2839 (2019).

41. Bailey, T. L., Johnson, J., Grant, C. E. & Noble, W. S. The MEME Suite. *Nucleic Acids Res.* **43**, W39–W49 (2015).

42. Quinlan, A. R. & Hall, I. M. BEDTools: a flexible suite of utilities for comparing genomic features. *Bioinformatics* **26**, 841–842 (2010).

43. Ray, D. *et al.* A compendium of RNA-binding motifs for decoding gene regulation. *Nature* **499**, 172–177 (2013).

44. Köhler, S. *et al.* The Human Phenotype Ontology in 2021. *Nucleic Acids Res.* **49**, D1207–D1217 (2021).

45. Black, B. L. & Olson, E. N. TRANSCRIPTIONAL CONTROL OF MUSCLE DEVELOPMENT BY MYOCYTE ENHANCER FACTOR-2 (MEF2) PROTEINS. *Annu. Rev. Cell Dev. Biol.* **14**, 167–196 (1998).
46. Jeronimo, C., Bataille, A. R. & Robert, F. The Writers, Readers, and Functions of the RNA Polymerase II C-Terminal Domain Code. *Chem. Rev.* **113**, 8491–8522 (2013).
47. Piva, F., Giulietti, M., Nocchi, L. & Principato, G. SpliceAid: a database of experimental RNA target motifs bound by splicing proteins in humans. *Bioinformatics* **25**, 1211–1213 (2009).
48. Das, S. & Chadwick, B. P. Influence of Repressive Histone and DNA Methylation upon D4Z4 Transcription in Non-Myogenic Cells. *PLOS ONE* **11**, e0160022 (2016).
49. Savarese, M., Sarparanta, J., Vihola, A., Udd, B. & Hackman, P. Increasing Role of Titin Mutations in Neuromuscular Disorders. *J. Neuromuscul. Dis.* **3**, 293–308 (2016).
50. Guo, W., Bharmal, S. J., Esbona, K. & Greaser, M. L. Titin diversity--alternative splicing gone wild. *J. Biomed. Biotechnol.* **2010**, 753675 (2010).
51. Fanin, M., Nascimbeni, A. C. & Angelini, C. Screening of calpain-3 autolytic activity in LGMD muscle: a functional map of CAPN3 gene mutations. *J. Med. Genet.* **44**, 38–43 (2006).
52. Pistoni, M. *et al.* Rbfox1 downregulation and altered calpain 3 splicing by FRG1 in a mouse model of Facioscapulohumeral muscular dystrophy (FSHD). *PLoS Genet.* **9**, e1003186 (2013).
53. Singh, R. K., Kolonin, A. M., Fiorotto, M. L. & Cooper, T. A. Rbfox Splicing Factors Maintain Skeletal Muscle Mass by Regulating Calpain3 and Proteostasis. *Cell Rep.* **24**, 197–208 (2018).
54. Wei, B. & Jin, J.-P. TNNT1, TNNT2, and TNNT3: Isoform genes, regulation, and structure–function relationships. *Gene* **582**, 1–13 (2016).

55. Sancisi, V. *et al.* Altered *Tnnt3* characterizes selective weakness of fast fibers in mice overexpressing FSHD region gene 1 (*FRG1*). *Am. J. Physiol.-Regul. Integr. Comp. Physiol.* **306**, R124–R137 (2014).

56. Gabellini, D. *et al.* Facioscapulohumeral muscular dystrophy in mice overexpressing FRG1. *Nature* **439**, 973–977 (2006).

57. Bouwman, L. F. *et al.* Dnmt3b regulates DUX4 expression in a tissue-dependent manner in transgenic D4Z4 mice. *Skelet. Muscle* **10**, 27 (2020).

58. Cheng, X. Structure and Function of DNA Methyltransferases. *Annu. Rev. Biophys. Biomol. Struct.* **24**, 293–318 (1995).

59. Duymich, C. E., Charlet, J., Yang, X., Jones, P. A. & Liang, G. DNMT3B isoforms without catalytic activity stimulate gene body methylation as accessory proteins in somatic cells. *Nat. Commun.* **7**, 11453 (2016).

60. Zeng, Y. *et al.* The inactive Dnmt3b3 isoform preferentially enhances Dnmt3b-mediated DNA methylation. *Genes Dev.* **34**, 1546–1558 (2020).

Figure S1

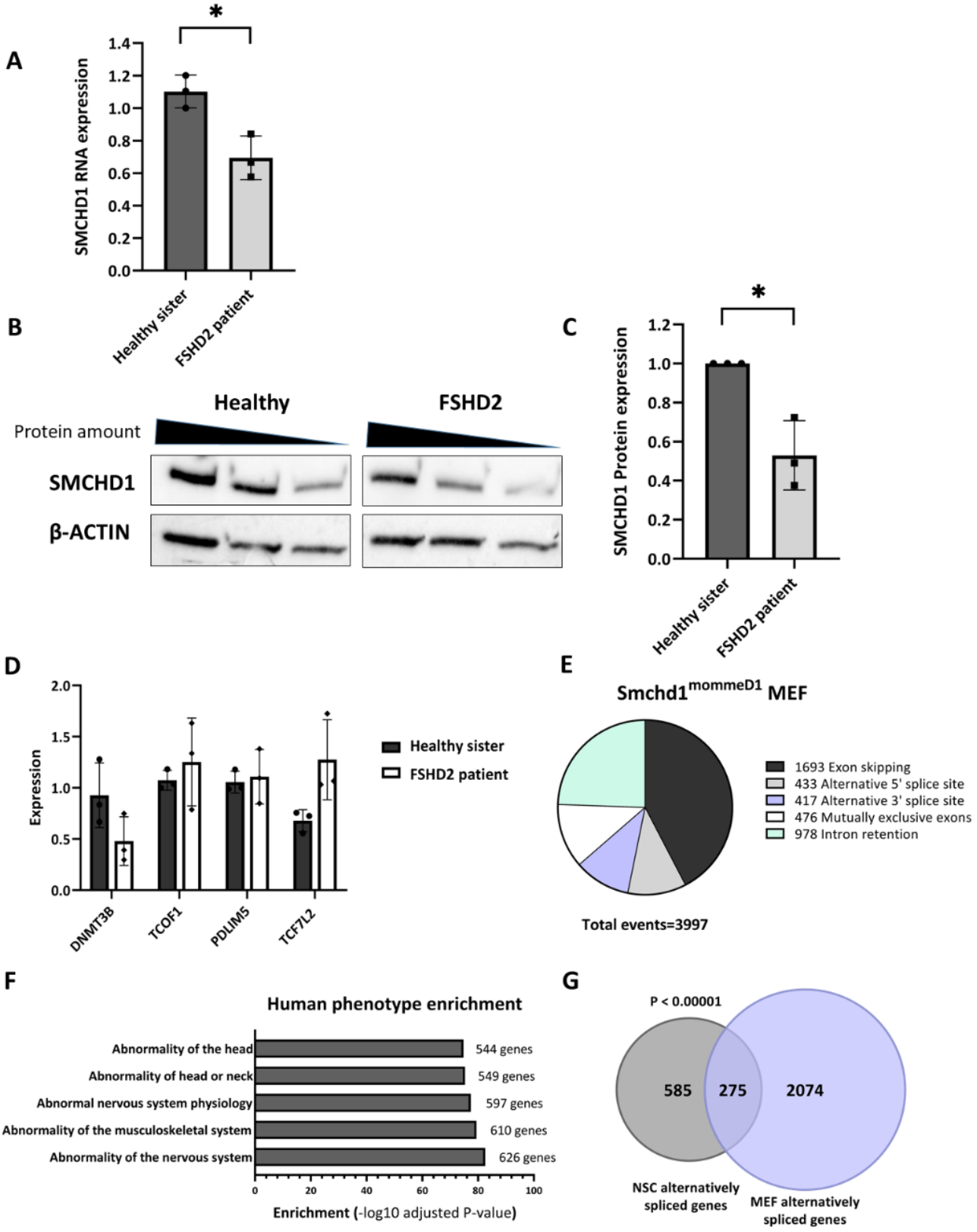

Figure S1. A-D. RNA was extracted from lymphoblasts of an FSHD2 patient and her healthy sister and analyzed by real-time PCR for *SMCHD1* total mRNA amount relative to *CycloA* reference gene (**A**). Protein was extracted and Western blot was conducted with the indicated antibodies (**B**). Quantification of Western blot (C). RNA was extracted and real-time PCR was conducted to the indicated gene relative to *CycloA* reference gene (**D**). Values represent averages of three experiments ±SD, [* p<0.05]. ***E-F.*** RNA-seq of Smchd1^{MommeD1} MEF samples was analyzed using rMATS (FDR<0.05). Proportion of each alternative splicing event is presented relative to WT **(E)**. Gene set enrichment for human phenotypes, enrichment significance represented as –log10 adjusted P-value **(F)** Summary of significant alternative splicing events (FDR<0.05) from the five subtypes identified by rMATS in Smchd1^{MommeD1} mice MEF RNA-seq data. ***G.*** Venn diagram presenting the overlap between Smchd1 alternative splicing regulation in NSC and MEF of Smchd1^{MommeD1} mice.

Figure S2

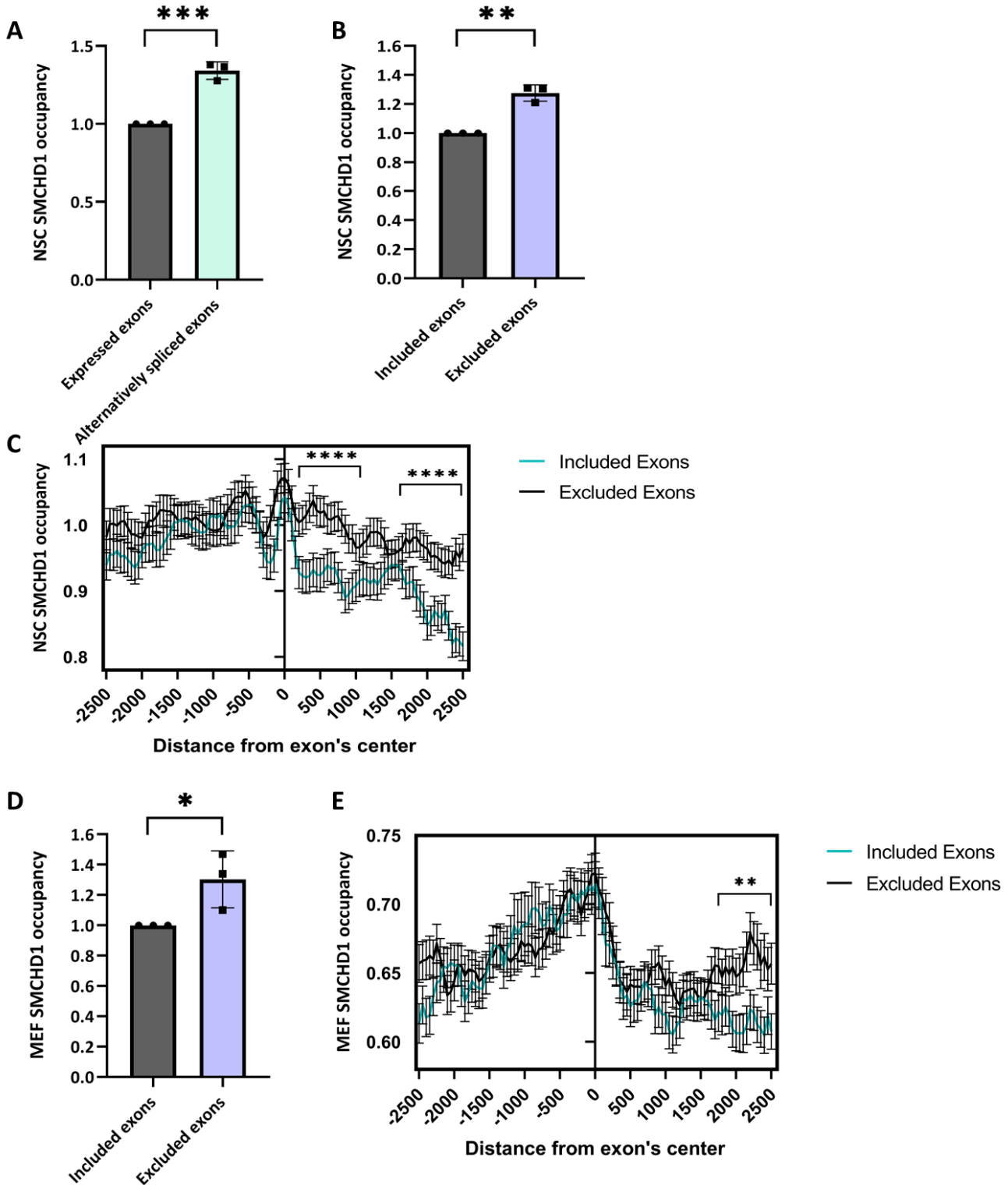

Figure S2

A-C GFP ChIP-seq in primary NSCs with endogenous Smchd1-GFP fusion protein. Smchd1 occupancy analyzed as the number of Smchd1 peaks present within 5kb of alternatively spliced or expressed (TPM>1) exons **(A)** or within 5kb of differentially included or excluded exons in Smchd1^{MommeD1} NSC **(B)** .Values represent averages of three ChIP-seq replicates from each cell type ±SD [* p<0.05; **p<0.01; ***p<0.001;]. Aggregation plot depicting the average normalized Smchd1 occupancy, at and near exons differentially included or excluded in Smchd1^{MommeD1} mice. X axis represent bins of size 50 bp around the center of the exon [****p<0.0001] **(C)**. ***D-E***. SMCHD1 ChIP-seq in MEFs. SMCHD1 occupancy analyzed as the number of SMCHD1 peaks present within 5kb of included or excluded exons in Smchd1^{MommeD1} MEF. Values represent averages of three ChIP-seq replicates from each cell type ±SD [* p<0.05; **p<0.01; ***p<0.001;] (A). Aggregation plot depicting the average normalized Smchd1 occupancy, at and near exons differentially included or excluded in Smchd1^{MommeD1} MEF. X axis represent bins of size 50 bp around the center of the exon [**p<0.01].

Figure S3

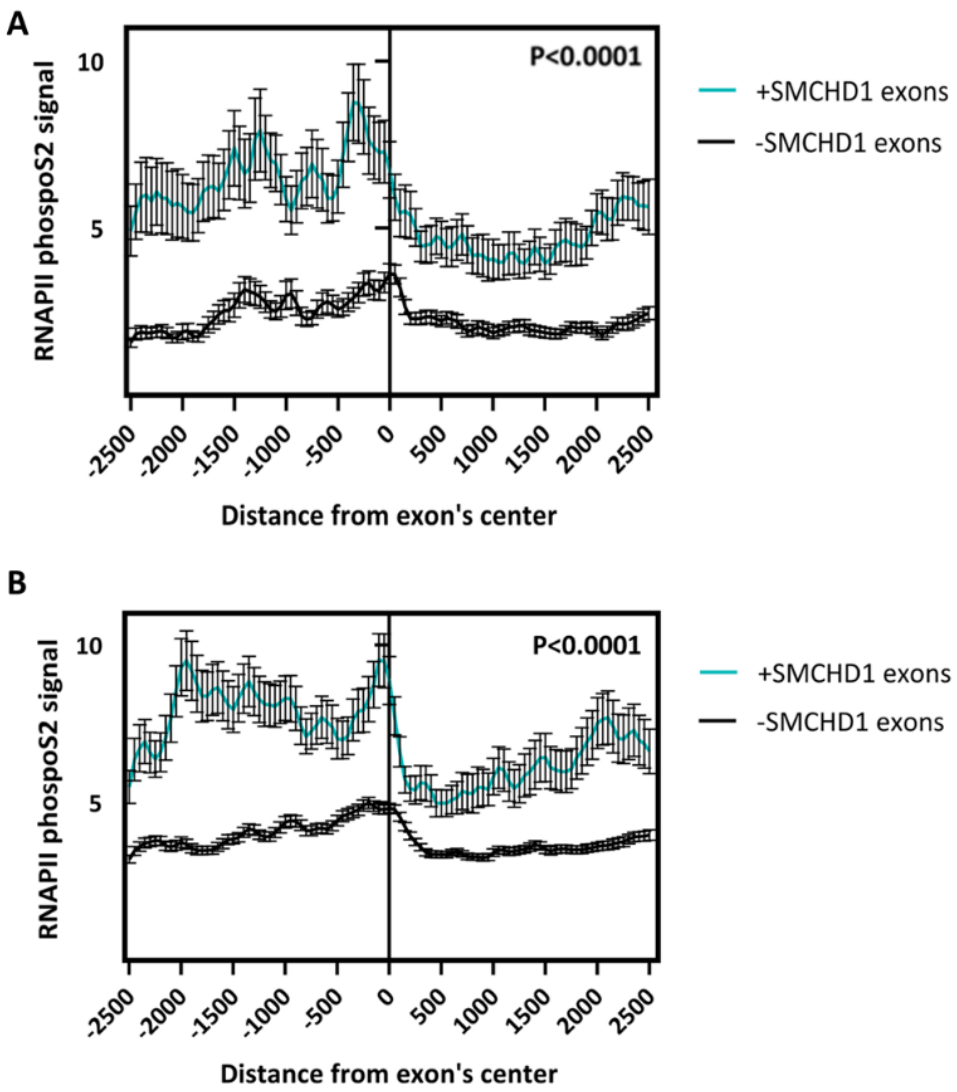

Figure S3

A-B. Aggregation plot depicting the average normalized phospho-Ser2 levels of RNAPII at and near alternatively spliced exons differentially bound by Smchd1 in NSC (A) or MEF (B). X axis represent bins of size 50 bp around the center of the exon .

Figure S4

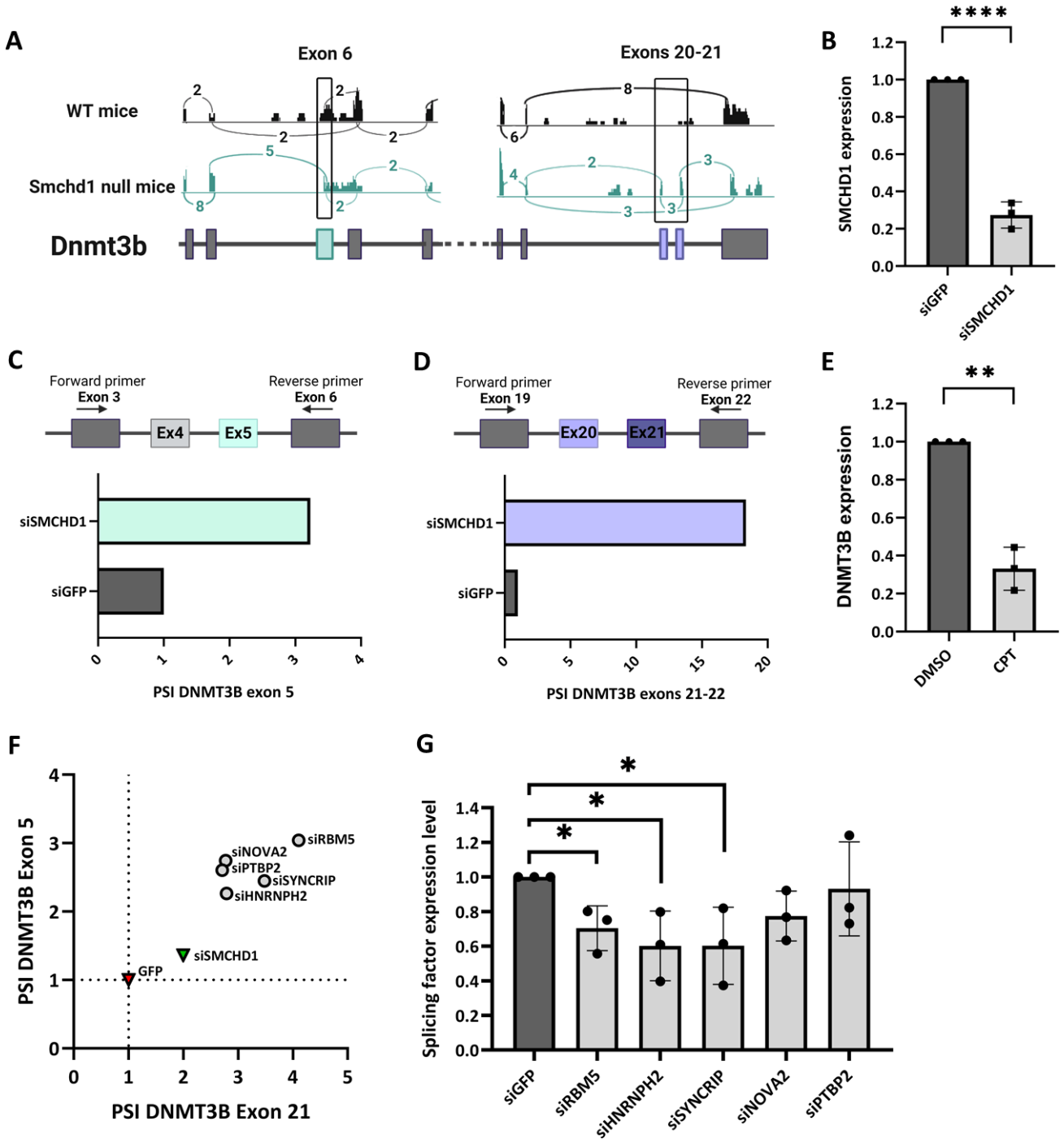

Figure S4

(A) RNA was extracted from three Smchd1^{MommeD1} mice NSC samples and two WT mice NSC samples. RNA-seq was conducted and analyzed using rMATS (FDR<0.05). Genome browser view of the Dnmt3b alternatively spliced junctions presented by sashimi plots, arcs denote splice junctions quantified in spanning reads. ***(B-D)*** HCT116 cells were transfected with siRNA targeting SMCHD1 or GFP as negative control. Total RNA was extracted and analyzed by real-time PCR for SMCHD1 total mRNA amount relative to *CycloA* reference gene. Values represent averages of three experiments done in triplicates ±SD normalized to negative control (siGFP) [****p<0.0001] (paired Student's t-test) **(B)**. Semi quantitative PCR was conducted for exons 4-5 **(C)** and exons 20-21 **(D)** using custom primers as described. PSI is calculated as the included product amount relative to the excluded product, and normalized to siGFP as a negative control. ***(E)*** HCT116 cells were treated with 6uM of CPT or DMSO as negative control for 6 hr. Total RNA was extracted and analyzed by real-time PCR for total DNMT3B mRNA amount relative to *CycloA* reference gene. Values represent averages of three experiments done in triplicates ±SD normalized to negative control (DMSO) [**p<0.01] (paired Student's t-test). ***(F)*** HCT116 cells were transfected with siRNA targeting 71 human splicing factor, SMCHD1 as a positive control and GFP as negative control. Total RNA was extracted and analyzed by real-time PCR for DNMT3B exon 5 and exon 21 relative to DNMT3B total mRNA amount. PSI was calculated as DNMT3B exon inclusion/DNMT3B total mRNA and normalized to negative control (siGFP). Values represent averages of two experiments ±SD. Negative control (siGFP) PSI is represented by the dotted line at 1. ***(G)*** HCT116 cells were transfected with siRNA targeting each splicing factor hit indicated or GFP as a negative control. Total RNA was extracted and analyzed by real-time PCR for splicing factor total mRNA amount relative to *CycloA* reference gene. Values represent averages of three experiments done in triplicates ±SD normalized to negative control (siGFP) [*p<0.05] (paired Student's t-test).

Figure S5

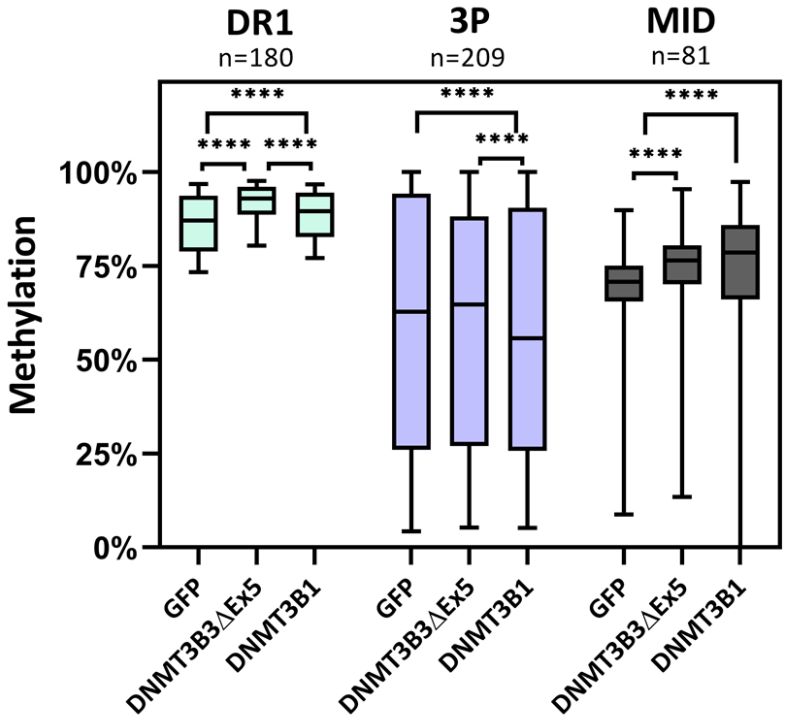

Figure S5

(A) DNMT3B null HCT116 cells were infected with empty-GFP, GFP-DNMT3B3ΔEx5 or GFP-DNMT3B1 lentiviruses. DNA was isolated and bisulfite converted. PCR was conducted in three locations along the D4Z4 region (see methods) and products were sequenced. Methylation level in each CG was assessed using Biscuit. Methylation level is presented at three different regions of D4Z4 region (see methods).